Stimulated raman adiabatic passage in optomechanics

Fedoseev, V.

6

Setup for optomechanical quantum experiments

In this chapter we discuss the optical setup that has been built, as well as new components that are still under construction, in our laboratory for quantum optomechanical experiments.

Full setup overview

Figure 6.1 presents a schematic overview of our setup for quantum optomechanical experiments involving mechanical state projection via detection of the Stokes and anti-Stokes scattered photons. Let's consider an example of a single-phonon state preparation considered in Chapter 4 as the first step for STIRAP of a quantum state. Experimentally we start from the mechanical mode being sideband cooled close to its ground state. Next, the cooling tone is switched off and a weak blue-detuned pump pulse is sent to the cryogenic cavity. With small probability the pulse will result in a Stokes photon. To separate the Stokes photon from the pump pulse the light leaking from the cavity is sent through a special optical filter. The filter consisting of 4 consecutive high-finesse cavities is resonant with the cryogenic cavity and thus the pump pulse is reflected from the filter cavities, while the Stokes photon is transmitted and then detected by a superconducting nanowire single photon detector (SNSPD).

The cryogenic cavity was described in the previous chapter.

In the first section the set of the filter cavities is discussed. These are four stable cavities of very similar design to the cryogenic cavity. These cavities are held in a room temperature vacuum chamber and the length of each cavity is controlled by a microprocessor within 5 pm. This work was done together with Sebastian ten Haaf [80] and Owen Huisman [81].

In the second section we describe the superconducting nanowire single photon detectors with $> 90\%$ detection efficiency and 10 mHz dark count rate installed in our dilution cryostat. This work was done together with Remi Claessen [82].

Kellan Colburn (UCSB) and Xinrui Wei also participated in the work presented in this chapter.

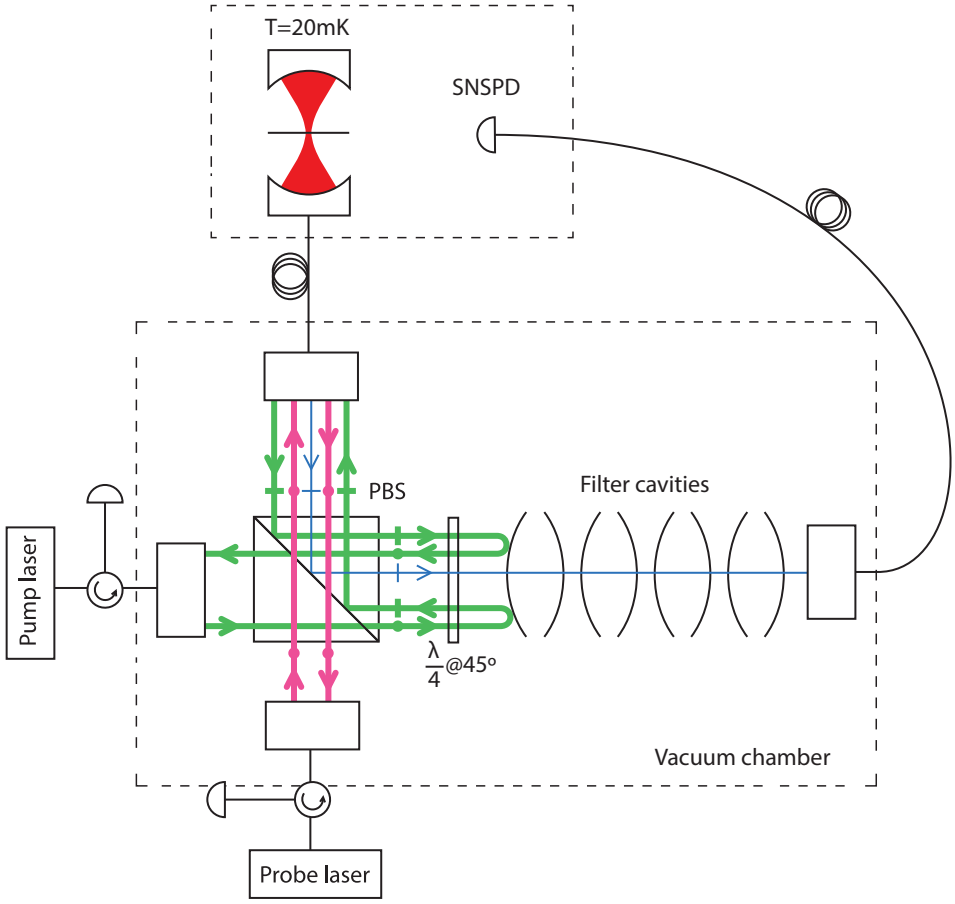

Figure 6.1: Schematics of a quantum optomechanical experiment with detection of a scattered heralding photon, depicted by the blue line. This design maximizes the transmission of the optomechanically scattered photons.

6.1 Filter cavities

6.1.1 Optical design

The inelastic scattering probability P_{scat} of a photon in a cavity with linewidth κ on a phonon is $\propto (g_0/\kappa)^2$, which is typically $10^{-8} - 10^{-6}$ [3, 66], where g_0 is the single-photon optomechanical coupling. Thus the scattered photon at frequency $\omega_{\mathrm{pump}} \pm \Omega_m$ is accompanied by order of $10^6 - 10^8$ pump photons at ω_{pump}, where Ω_m is the mechanical oscillator frequency. Observation of the scattering event re-

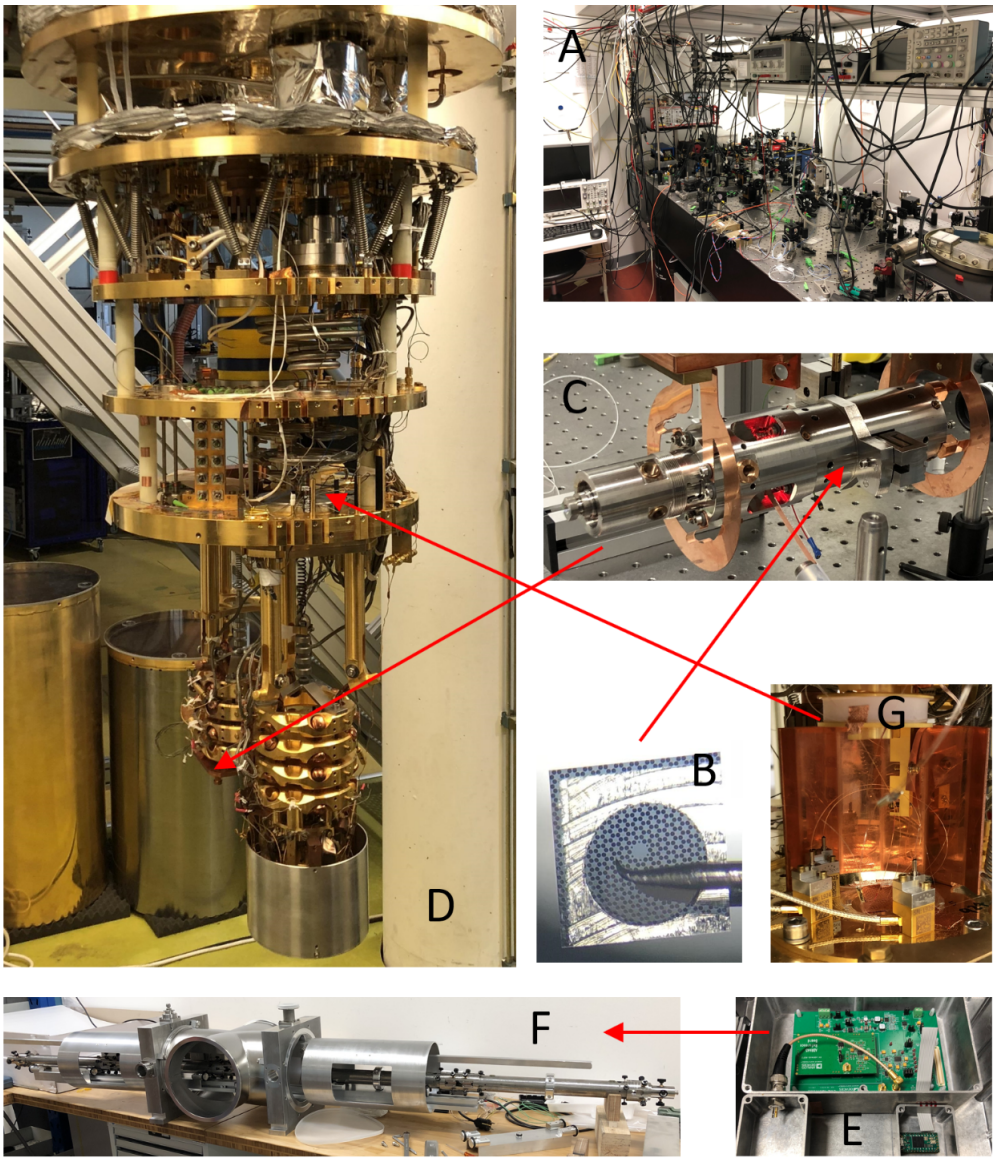

Figure 6.2: All components of the experiment: optical table with lasers (A), membrane (B), cryogenic cavity (C), ultra-low vibration due to the spring-mass mechanical filter dilution cryostat with a nuclear demagnetization stage reaching 1 mK (D), microprocessor control with a low noise digital to analog converter (E) for the filter cavities system (F), single photon detectors (G).

quires an optical filter capable of attenuating the light fields detuned from the filter transmission frequency by Ω_m by much more than $1/P_{\mathrm{scat}}$.

For optomechanical devices operating in the MHz regime it is a challenge to build

such a filter. For example, this would require a Fabry-Perot cavity with a linewidth of ~ 1 Hz causing a delay of about 1 second. In the presence of the cooling light tone the linewidth of the originating anti-Stokes photons will be equal to $\Gamma_{\rm opt} + \Gamma_m$ which is of the order of 100 Hz. Therefore, these photons will be transmitted through the filter with probability ~ 0.01 or less. Another consideration is stability: it is challenging to keep various optical components on resonance with precision of 1 Hz. Nevertheless, the required filter performance can be achieved by concatenating few Fabry-Perot cavities [66].

We adapt and significantly improve upon the filter design presented in [66]. Our filter consists of four consecutive Fabry-Perot cavities (Fig. 6.3) with a linewidth of 30 kHz each. The design transmission of the filter on resonance is ~ 0.85, which is determined by absorption and scattering in the dielectric coatings of the Bragg mirrors and residual reflection from the anti-reflection coatings of the lenses and backside of the mirrors. To achieve this high overall transmission the coatings with < 3 ppm scattering and absorption loss are required. We believe this can be achieved by state of the art supermirrors. We ordered superpolished substrates with surface roughness < 0.1 nm RMS (measured with white light interferometer) and the coatings were deposited using the ion beam deposition technique.

The design filter transmission of light fields detuned by 1 MHz is $< 10^{-14}$, see Fig. 6.4. We consider two optical arrangements with (red lines) and without back-reflection (blue lines) between the cavities.

In the first arrangement there are optical isolators (dotted boxes) making the cavities independent and the overall filter transmission equal to the product of each cavity transmission (red curves on Fig. 6.4). The first optical isolator consists of a polarizing beam splitter (PBS) and a $\lambda/4$ wave-plate at 45^o and accepts linearly polarized light. Light in each cavity is circularly polarized, thus all the subsequent isolators include an extra $\lambda/4$ wave-plate. Altogether there are 26 surfaces in the optical isolators and special care was taken to achieve high transmission through this system. A company Union Optic agreed to pick the best set of the required optical components from their stock achieving the overall transmission of 96% through the whole system of optical isolators (as measured). The overall transmission of the filter is independent of the distance between each two cavities due to the isolators.

If the inter-cavity isolators are removed then the light back-reflected from a cavity starts to interfere with the previous cavity, thus the overall transmission becomes dependent on all the distances between the mirrors. This case was carefully evaluated in [80]. It appears that the transmission as a function of the light detuning Δ can be made $1 - (\Delta/\Delta_0)^8$ for small detuning values $|\Delta/\Delta_0| \ll 1$ having ba-

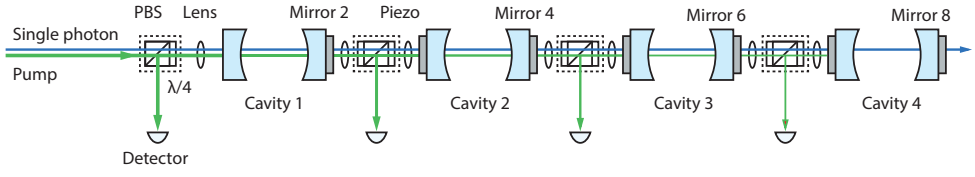

Figure 6.3: Optical setup of the filter. Only Stokes or anti-Stokes photons are transmitted.

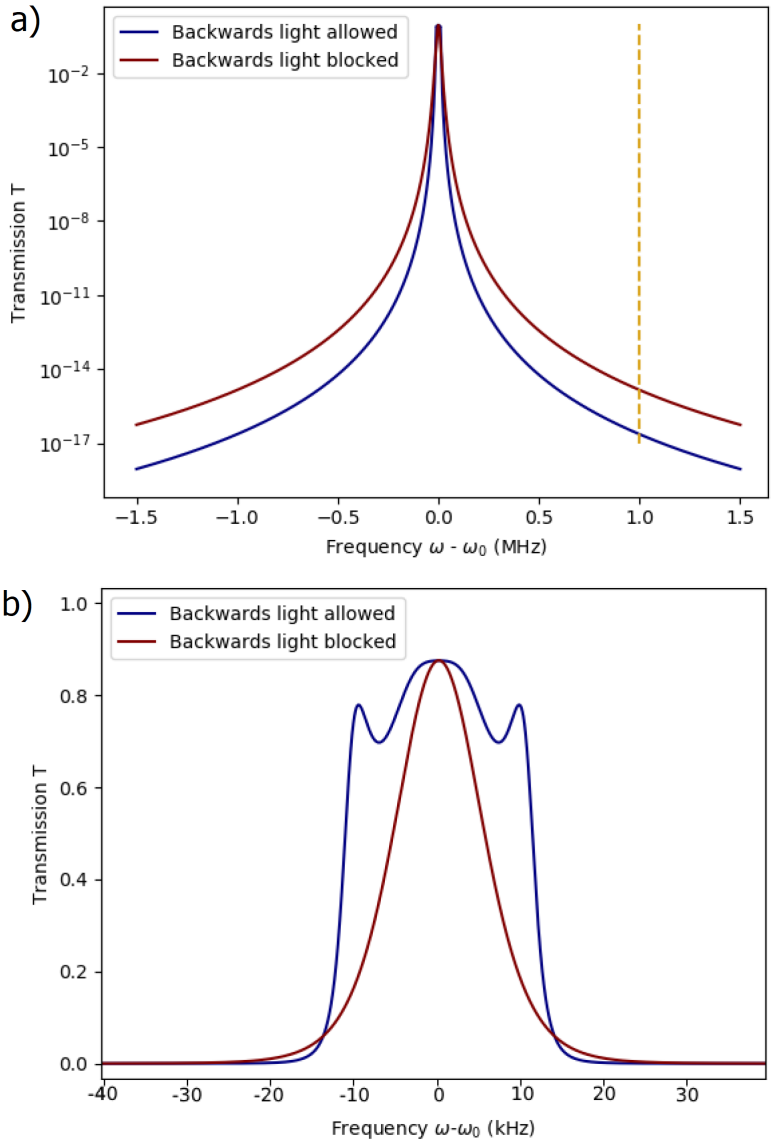

Figure 6.4: Filter transmission with optical isolators (red) and without optical isolators (blue). To achieve the transmission given by the blue line the inter-cavity distances must be controlled within 10 nm. a) shows the transmission for detunings less then 1.5 MHz on a logarithmic scale, b) shows the transmission for detunings less then 40 kHz on a linear scale.

sically a flat top, where Δ_0 is approximately the linewidth of an individual cavity. To achieve this the reflectivities of the mirrors should have specific values with $R_1 = R_8 < R_2 = R_7 < R_3 = R_6 < R_4 = R_5$, where R_i is the reflectivity of mirror

i. Another requirement is that the inter-cavity distances must be set to $n\lambda/2 + \lambda/4$ within 10 nm, where n is an integer number. If the reflectivities are restricted to be equal to have a single coating run, then the transmission curve looses its flat top as shown in Fig. 6.4b). Nevertheless, compared to the case of the system with optical isolators this case has three advantages:
- transmission on resonance is higher due to absence of the loss in the isolators;
- transmission in the vicinity of the resonance is significantly higher. This is beneficial if a scattered photon has some linewidth broadening and/or has random detuning from the resonance due to frequency noise;
- attenuation at 1 MHz detuning is ~ 100 stronger.
The price to pay is that the intercavity distances must be $n\lambda/2 + \lambda/4$ within ~ 10 nm, where n is an integer number. Another, significant complication is the aligning procedure and keeping the cavities resonant to a given frequency.

The filtering system with isolators can be aligned and locked on resonance sequentially using the dither locking technique as the cavities are independent. In the configuration without isolators case the alignment difficulty can be seen from the following. Let's assume the mode matching for the filter cavities is in place and the goal is to keep the four cavities resonant with the laser light. Let's consider mirrors having arbitrary z-axis shifts on the wavelength scale from the optimal resonant configuration. In the case of ideal mirrors with no absorption loss sweeping position of any mirror will have hardly any effect on the reflection signal for almost all mirror positions except for the resonant case of all the four cavities as 100% of light is reflected if at least 1 cavity is off-resonance.

We expect the following alignment procedure to work in the case of no isolators and non-ideal mirrors. For the initial mode matching alignment the cavities might be made independent by inserting optically thin isolators (true zero order $\lambda/4$ wave-plates and film polarizers). After alignment the isolators can be removed not disturbing the mode matching. Alternatively S.L.D. ten Haaf proposed a procedure of making the cavities resonant and setting the proper inter-cavity distances. The procedure is based on non-zero absorption in mirror coatings and can be understood from the following observation. Let's start from arbitrary mirrors positions on the wavelength scale. Simulations show that when mirror2 (see Fig. 6.3) position is swept a measurable reflection dip can be observed when cavity1 becomes resonant with the laser light, Fig. 6.5a). In this case light can propagate further to the space between cavity1 and cavity2 and part of the light is lost due to resonance in cavity1 with absorptive mirrors. The value of this reflection dip is proportional to the absorption loss in the coatings. Next, cavity1 is assumed to be locked on its resonance. A position sweep of Mirror3 has two features, Fig. 6.5b): the reflection signal has a periodic term due to the dependence of the effective reflectivity of the system of mirror2-mirror3 on the distance between these two mirrors and a resonance dip due to cavity2 becoming also resonant with the laser light. It appears that all four cavities can be made resonant and the inter-cavity distances can be set to $n\lambda/2 + \lambda/4$ exploiting similar effects as shown in Fig. 6.5.

Keeping all four cavities on resonance is also a non-trivial task. Modulating mirror2, mirror4, mirror6 and mirror8 positions at different frequencies and demodulating the overall reflection signal at these frequencies provides partial derivatives

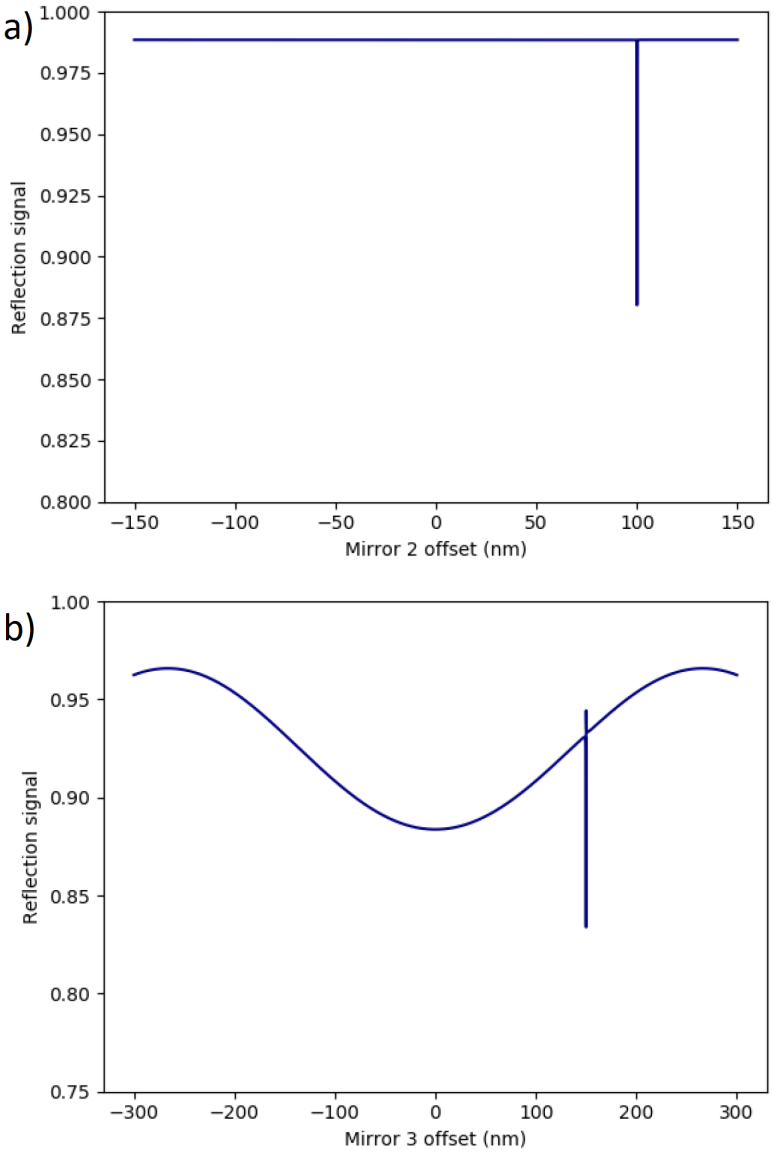

Figure 6.5: Filter reflection when the inter-cavity isolators are removed. a) Mirror2 position sweep with arbitrary other mirrors positions. Mirrors are numbered from left to right, see Fig. 6.3. b) Mirror3 position sweep with cavity1 resonant with the laser light and arbitrary other mirrors positions.

$\frac{\partial R}{\partial L_i}$, where R is the reflection signal and L_i are the i-th cavity lengths. In the configuration with isolators present the values of the derivatives give us full information on how to adjust each mirror position as the shift of mirror i from the ideal position

is directly proportional to $\frac{\partial R}{\partial L_i}$. To achieve the highest transmission of the laser to which the filter cavities are locked all mirrors must be set to their ideal positions, defined such that each individual cavity is on resonance with the incoming light fields. For any other mirrors positions the transmission will be lower. Situation is different in the configuration with no isolators. It appears, that if mirror2 is shifted from the ideal position, the transmission of the laser to which the filter cavities are locked can be restored to practically the same value as the transmission for the case with all mirrors at their ideal positions by adjusting the position of mirror4!

Simulations showed that the second derivatives matrix $\frac{\partial^2 R}{\partial L_i \partial L_j}$ is degenerate in the vicinity of the ideal mirrors positions. This means that observation of the partial derivatives $\frac{\partial R}{\partial L_i}$ does not provide the values ΔL_i - shifts of mirrors 2, 4, 6 and 8 to be corrected. This can be seen from

$$\frac{\partial R}{\partial L_i}(\Delta L_i) = \sum_{j=1}^{4} \frac{\partial^2 R}{\partial L_i \partial L_j} \Delta L_j. \tag{6.1}$$

The vector ΔL_i is not unique because $\left(\frac{\partial^2 R}{\partial L_i \partial L_j}\right)^{-1}$ is not defined. Simulations of a PID control keeping $\frac{\partial R}{\partial L_i} = 0$ shows that the lengths of the cavities do not converge to the mirrors configuration with $\Delta L_i = 0$, see Fig. 6.6. This confirms that there are non-zero mirrors position shifts ΔL_i for which $\frac{\partial R}{\partial L_i} = 0$.

Two solutions to this very challenging problem have been proposed. In the first one the shape of the transmission curve is taken as an additional input and a trained neural network finds the resonant situation for all four cavities. The second one is based on mechanical insertion of the inter-cavity isolators to make the cavities independent, adjust the cavity lengths appropriately and remove the isolators afterwards every few seconds. This can be achieved by a mechanism with step motors placing the isolators on the optical path and removing them after a short time enough for readjustment.

6.1.2 Mechanical design of filter cavities

The mechanical design is based on the cryogenic cavity design (see Fig. 6.7) as it demonstrated an ability to reach 96% optical coupling to a single mode fiber and very stable in time performance (optical coupling deteriorates by less than 1% during a couple of months at room temperature). The cryogenic cavity and the filter cavities together with its support were developed in close collaboration with Harmen van der Meer at the fine mechanical department of LION.. The fiber incoupling module and the first cavity are identical to the cryogenic cavity except for the cavity being 40 cm long. Each inter-cavity module holds 2 mode-matching lenses and an optical isolator ($\lambda/4$ waveplate at 45^o, PBS, $\lambda/4$ at waveplate 45^o). The light reflected from the next cavity is reflected by the PBS cubes and monitored by the photodiode.

In Fig. 6.1 all the four ports of the first PBS are used, this is planned to be implemented in the next iteration of the filter cavities system.

The whole setup of the filter cavities is about 2 m long and 5 cm in diameter resulting in high aspect ratio, thus it cannot be supported at two points. Multiple

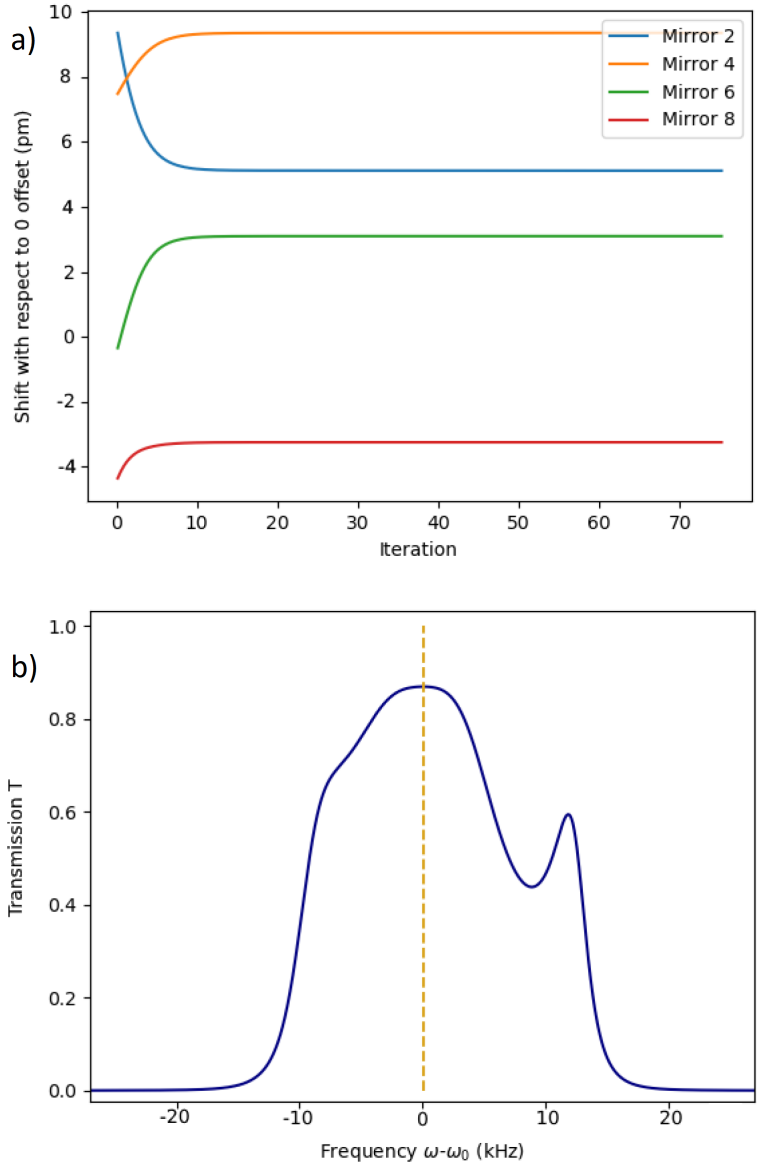

Figure 6.6: PID feedback control starting from a random state with non-zero demodulated signal proportional to $\frac{\partial R}{\partial L_i}$ and adjusting ΔL_i to reach a state with $\frac{\partial R}{\partial L_i} = 0$. a) The derivatives converge to 0. b) The total transmission of the final state.

point support is also not ideal as any aging effect in the support (rubber parts for example) will lead to support force redistribution and bending of the whole structure and misalignment as a result. To address these issues we developed a special support designed to hold each cavity with a constant force, see Fig. 6.8. The support

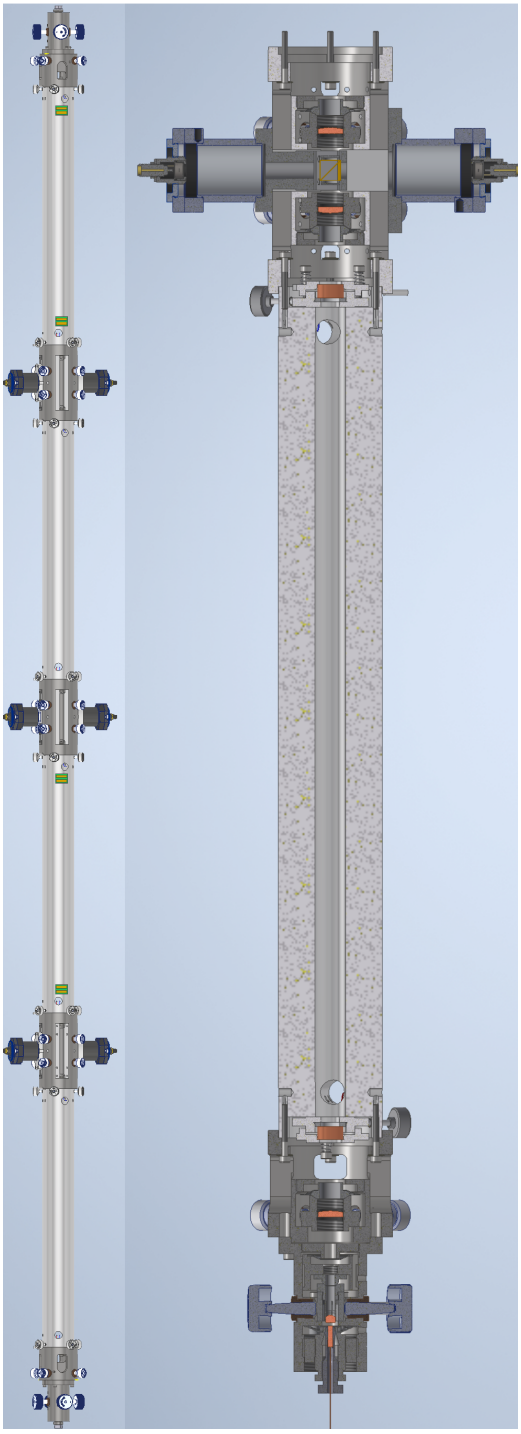

Figure 6.7: Mechanical design of the filtering cavities. All four cavities are arranged consecutively, left sketch. Right sketch shows the fiber incoupling together with the first cavity and an intercavity module containing mode matching lenses and an optical isolator.

consists of multiple moving parts connected by rubber rings. Rubber rings serve as springs with damping to create a multi-stage mechanical low pass filter. Each cavity is supported by an A-type piece held by B-type pieces in their centers such that A parts can rotate. The same holds for B parts. By design the force at all points holding the cavities are equal which is easy to see considering torque balance in the system. As a result if some rubber joint shrinks due to aging the whole system will adjust itself to restore the torque balance via force equality. We believe that this design of the support should benefit to the time stability of the optical alignment.

Figure 6.9 shows a photo of the filter cavities system together with the support assembled without optics. The C-type part is fixed inside the central part of the vacuum chamber, the B-type parts are represented by the two pieces of a tube with openings. The four A-type parts are also partly visible on the photo. After the optical alignment is done two large vacuum caps are attached from the sides and pressed against the large o-rings visible on the photo. The central part is closed by two blank flanges. Vacuum is maintained by an ion pump. There is a vacuum feedthrough for the fibers. The fiber going to the single photon detector is placed in a vacuum tight system of tubes connecting the filter vacuum chamber and the cryostat to ensure complete stray light isolation.

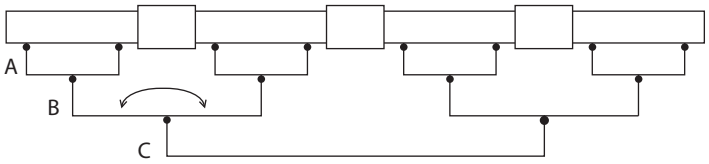

Figure 6.8: Constant force support design. The black circles represent joints free to rotate as shown by an arrow. The C part is fixed. Two B parts and four A parts can be rotated around their centers. This design ensures equal force support at each point holding the cavities.

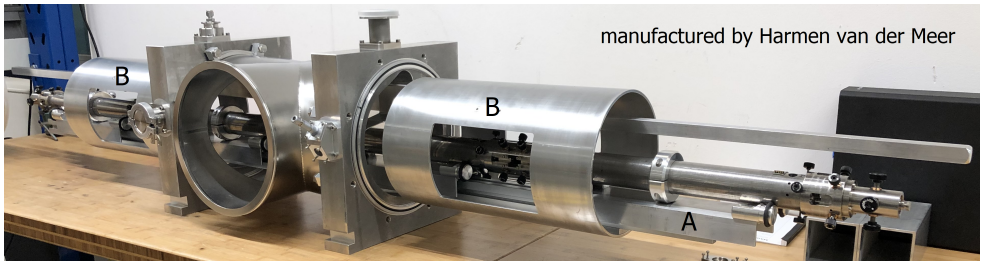

Figure 6.9: Photo of the support for the filter cavities holding the filter cavities. Each cavity is supported at two points of contact (black rubber rings) one of them is visible on the right side of the most right cavity. Moving parts A type and B type corresponding to Fig. 6.8 are marked with letters A and B. The C part is fixed to the central part of the vacuum chamber visible on the photo. After optical alignment is done vacuum caps are added on both sides to the large o-rings visible on the photo.

6.1.3 Control design

During the actual experiment we want to monitor for optomechanically scattered photons, thus the filter cavities must be resonant with these photons. To keep the filter cavities resonant some probe light should be transmitted through these cavities to monitor and subsequently being able to piezo adjust their lengths. But any transmitted light will reach the single photon detector, so these two requirements cannot be fulfilled simultaneously. Thus the experiment is organized in cycles: during the first part of each cycle (~ 0.1 s) the optical path towards the single photon detector is blocked not to blind the detector and the filter cavities are made resonant at the frequency of interest; during the second part of each cycle the feedback for filter cavities is frozen, the cavities probe light is switched off and the blocking is removed for optomechanical measurements (~ 1 s).

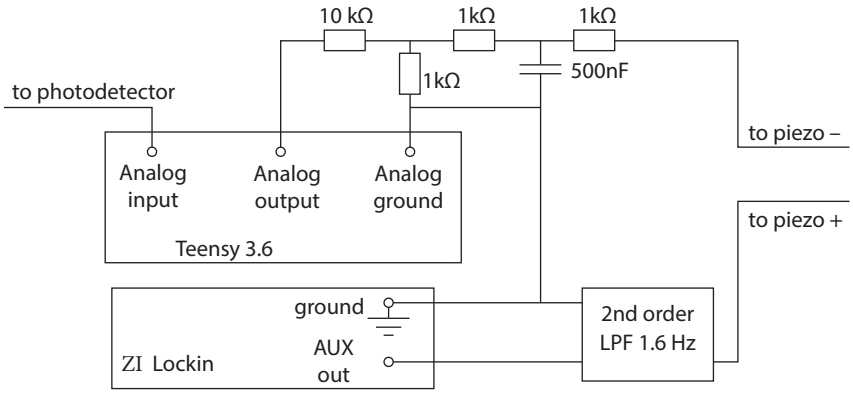

Figure 6.10: Electronic circuit used to keep each filter cavity locked to the laser light frequency. The Teensy 3.6 microprocessor modulates the piezo, demodulates the reflection signal and provides PID feedback signal.

In the actual experiment there are the following components which should be frequency locked: cryogenic cavity, filter cavities, probe and pump laser light fields. One possibility is to lock all the components to the cryogenic cavity as it might seem to be the quietest. But it is not the case: the pulse tube shakes the whole cryostat and modulates the cryogenic cavity resonance frequency by ~ 300 kHz (~ 0.1 nm) at multiple frequencies. The goal is to be able to freeze the feedback signal keeping the filter cavities resonant to the cryogenic cavity. The cryogenic cavity can be probed at all times, while the filter cavities cannot be observed during the collection of Stokes and anti-Stokes photons. Therefore we decided to introduce a stable narrow-linewidth reference cavity to which everything is locked. In the Fig. 6.12 we show that we indeed can freeze the feedback signal to filter cavities and they remain resonant with the reference cavity during a couple of seconds.

First, the probe filter cavity laser is locked to this reference cavity (9 kHz linewidth) via Pound-Drever-Hall technique.

Next, we demonstrate locking of a single test filter cavity (~ 20 kHz linewidth) to the reference cavity. The reference cavity and the test cavity are in separate vacuum

chambers. The locking is achieved by the dither locking technique: the length of the cavity is modulated by a piezo at 2 kHz, reflection signal is demodulated at the same frequency resulting in the derivative of the reflection signal with respect to the cavity length. This demodulated signal is used as an error signal for a PID feedback control. All these steps are done by a microprocessor connected to analog to digital (ADC) and digital to analog (DAC) converters [81]. The main requirement is that we should be able to scan 1 FSR (~ 50 V on piezo) and the voltage on the piezo should be stable to within a fraction of the filter cavity linewidth (~ 50 μV on piezo) during the freezing stage to guarantee close to unity transmission.

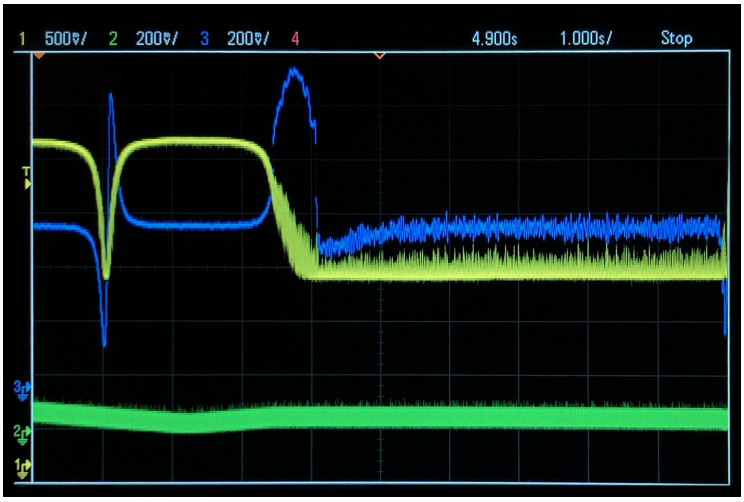

Figure 6.11: Locking a single test filter cavity with linewidth of ~ 20 kHz. Yellow trace shows reflection signal, blue trace shows the demodulated signal (PID error signal) and green trace shows the microprocessor output voltage before filtering and attenuation. First the voltage is swept across the cavity resonance, then the direction of the voltage change is reversed. When the reflection signal drops below a certain threshold approaching the cavity resonance, the rate of the voltage change is decreased 10 times. When the reflection signal reaches the next threshold the scanning is switched off and the feedback control is enabled.

In this proof of principle experiment we use a DAC of a Zurich Instruments lock-in as a source of stable voltage having a voltage range of -10..10 V. It's enough for a single cavity as it's always possible to find such a resonance of the reference cavity that the required voltage on the piezo of this test cavity is within range due to the cavities having different lengths (20 cm and 7 cm). This voltage is applied to the positive lead of the test cavity piezo passing through a low-pass filter, see Fig. 6.10. For this test we are using a Teensy 3.6 microprocessor having built-in 14 bit ADC and DAC with a range from 0 to 3 V for both of them. We assume that the noise of this DAC is of the order of the least significant bit (LSB), which is 200 μV. To satisfy our requirement for voltage stability of 50 μV we use a voltage divider 1:10 consisting of 1 kΩ and 10 kΩ resistors. This brings the low frequency noise of the DAC down to ~ 20 μV. This signal is sent to the negative lead of the piezo after passing through another low-pass filter (2nd order with the corner frequency of 20 Hz).

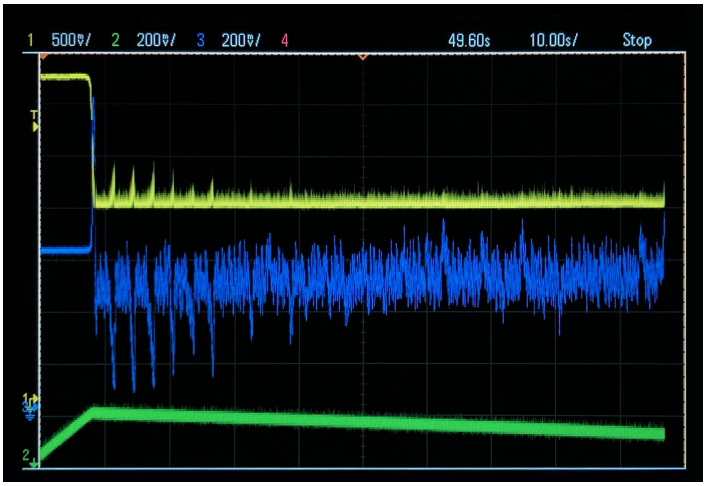

Figure 6.12: Repetitive cycles of 2 s locking and 1 s freezing the feedback voltage. During the first few cycles the system drift is not compensated, which is visible during the PID freeze states when the error signal monotonically decreases. Another PID feedback compensates for the drift. Just after locking the drift is not fully compensated as the integral part of the PID has not reached the steady state yet. The drift becomes fully compensated after $\sim$ 1 minute. The system reaches the steady state after $\sim$ 10 minutes.

Modulation signal of $\sim$ 50 μV pk-pk at 2 kHz is applied to the negative piezo lead, reflection light is detected by a photodetector, its output is sent to the ADC of the microprocessor. The demodulated signal is shown on Fig. 6.11 by the blue trace. The oscilloscope operates in the peak-detect mode. Here the cavity is scanned first, and then the PID feedback is switched on when the reflection signal is close to its minimum value.

Next we realize the freeze-lock cycles. After each lock period of 2 s the PID feedback is frozen for 1 s, see Fig. 6.12. Significant drift is present in the frequency difference of the filter cavity and the reference cavity which is visible in the first few lock-freeze cycles. To compensate for this drift another PID loop is realized (with an integral component only) which takes the first PID correction signal accumulated over a cycle as an error signal. This double-integrating scheme is able to keep the test filter cavity on resonance with the reference cavity for at least 30 s in this compensated freeze state.

To improve the transmission of the filter cavity even further and to cover the full FSR we will use a state-of-the-art 20 bit DAC instead of the built-in Teensy 3.6 DAC for the fine control of the piezo voltage and another 20 bit DAC output amplified 3 times using a zero drift operational amplifier for the coarse voltage control.

6.2 Single photon detectors

Scattered photons created in the optomechanical interaction inside the cryogenic cavity, travel through the filter cavities and finally are detected by a superconducting nanowire single photon detector (SNSPD). We tested four SNSPDs purchased from Photon Spot, optimized for 1064 nm. Each detector contains a SiW nanowire having a meander shape and covering an area of 20x20 μm^2. The bias current is sent through the DC port of a bias-T to the nanowire so that the nanowire is in the superconducting state close to its critical state. Absorption of a photon by the nanowire leads to creation of a hotspot - a small region with non-equilibrium state of electrons. This does not happen by direct heating above the critical temperature [83]. This breaks the Cooper pair locally creating a non-superconducting island in the nanowire. This, in turn, increases the current density above the critical value in the remaining superconducting part around the hotspot which in the end makes a piece of the nanowire to be in the normal state. This leads to an abrupt increase of the nanowire resistance to about 1 $k\Omega$ creating a voltage spike due to the nanowire inductance. The voltage spike travels to the bias-T and exits through its radio frequency port and is subsequently amplified and measured, see Fig. 6.13.

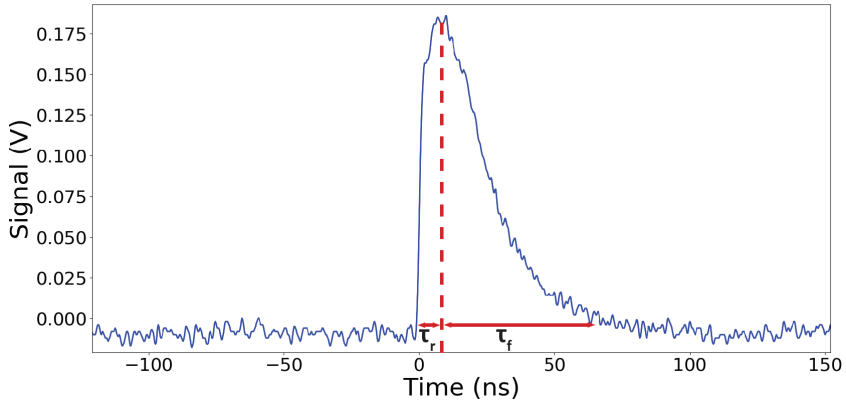

Figure 6.13: Signal resulting from detection of a single photon. Rise and fall times are denoted by arrows.

The detectors were installed in the cryostat and were calibrated using the procedure described in [84]. Laser light was split by a calibrated beamsplitter (BS). One output of the BS was measured by a powermeter, the other output was sent through two electronic variable optical attenuators to each detector. The BS and attenuators were single-mode fiber coupled. The detection efficiency of three detectors was measured as a function of the bias current, see Fig. 6.14. The system detection efficiency (SDE) is defined as the ratio of the number of clicks produced by the detection electronics and the number of photons entering the fiber attached to the detectors. Two detectors were measured to have SDE of the exceptional value of $95\% \pm 7\%$, and one of them will be used in the future quantum optomechanical experiments.

Another important characteristics of a single photon detector relevant to the pro-

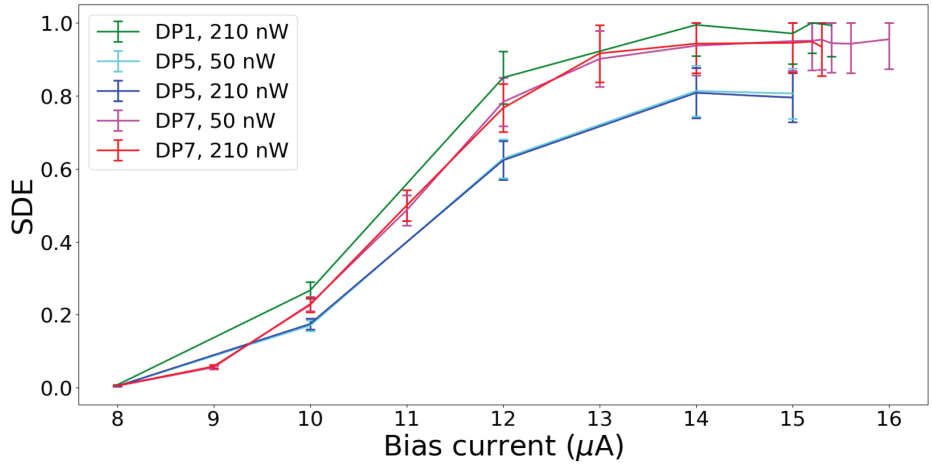

Figure 6.14: Measured system detection efficiency of superconducting nanowire single photon detectors. The efficiency depends on the bias current flowing through the nanowire. The detectors were illuminated by two different light intensities, 50 nW and 210 nW before the attenuation or $\sim 0.5 \times 10^5$ and $\sim 2 \times 10^5$ photons per second on the detectors.

tocol described in Chapter 4 is the dark count rate (DCR), meaning the rate at which a detector clicks without photons to be detected launched into the fiber. These detectors appeared to be extraordinary also from this point of view. The fourth detector was kept in the dark (no fiber attached) thermalized at 20 mK. The dark count click rate is ~ 0.3 mHz - on average we observed ~ 1 click per hour. The other three detectors with optical fibers leaving the cryostat were measured to have DCR of ~ 10 mHz. The increased DCR of these detectors might be explained by the black body radiation of the fiber segments kept at room temperature. We found that the click rate we were detecting with no light sent to the detectors heavily depended on the shielding of the detector fibers from the stray light. The smallest rate of DCR (~ 10 mHz) was observed when the fibers leading to the detectors were placed in a vacuum-tight metal tubing outside the cryostat. This guaranteed no stray light entering the fibers.

Acknowledgements

The results in sections 6.1.1 and 6.1.2 are part of the M.Sc. thesis of S.L.D. ten Haaf. The research was conducted together with and under the daily supervision of Vitaly Fedoseev. Figures 6.4, 6.5 and 6.6 were prepared by S.L.D. ten Haaf.

The results in section 6.1.3 are part of the B.Sc. thesis of O. Huisman. The research was conducted together with and under the daily supervision of Vitaly Fedoseev.

The results in section 6.2 are part of the M.Sc. thesis of R. Claessen. The research was conducted together with and under the daily supervision of Vitaly Fedoseev. Figures 6.13 and 6.14 were prepared by R. Claessen.